Towards Lossless Plasmonics

Master Thesis

Leiden University

Quantum Optics group

Author:
Ralph Lenssen

Supervisor:
Martin van Exter
Frerik van Beijnum

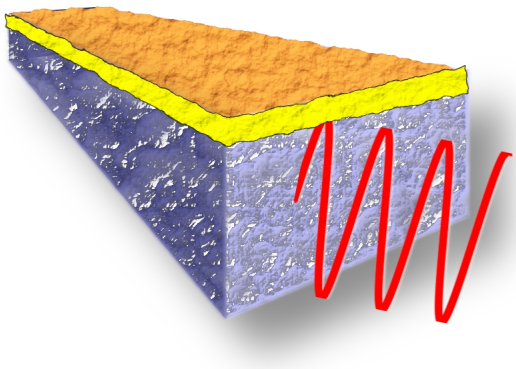

December 25, 2011

Abstract

Surface plasmons are modes of electromagnetic radiation that propagate along the interface of a metal and a dielectric material. They suffer large losses due to the absorption of the metal, limiting their propagation length. This thesis discusses whether this propagation length can be increased by replacing the dielectric by a gain medium.

The metal has a hole or slit array structure in the surface to couple out plasmons. In the spectrum of the out-coupled light, Rayleigh and plasmon resonances are found. These resonances are studied at different angles and with different gain. The widths of the resonances indicate that the gain material has increased the propagation length of the plasmons to 3 μm.

Contents

Chapter 1

Introduction

This section first explains what a surface plasmon is and introduces the idea of lossless plasmonics. Then, a historical overview of the field of plasmonics is provided, including a discussion of other related research. At the end a general outline of this thesis can be found.

1.1 Surface plasmons and our goal

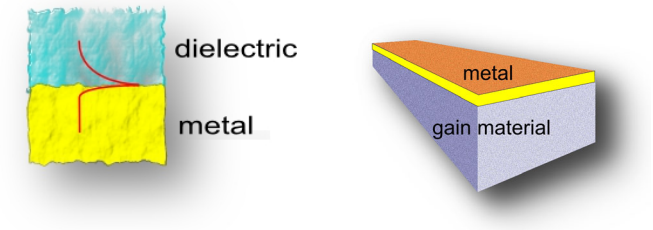

(a) (b)

Figure 1.1: *Figure (a) shows a schematic image of a surface plasmon. The red line indicates the magnetic field of the plasmon. Figure (b) illustrates how the propagation length is improved by sticking a gain layer to a metal surface.*

Surface plasmon polaritons are modes of electromagnetic radiation that are confined to the interface of a metal and a dielectric material. The amplitude of the magnetic field of the plasmon decreases exponentially in the directions perpendicular to the surface, as shown in figure 1.1(a). In this thesis we will call these modes plasmons, not to be confused with the excitation of bulk plasmon in a metallic volume.

Plasmons suffer large losses from the absorption of the metal, limiting their propagation length. The aim of our research is to increase the propagation length of plasmons and to explore the possibility of lossless plasmons. This will be done by adding a gain material to the metal surface, as shown in figure 1.1. Plasmons are created by the fluorescence emitted by the gain layer. The plasmons are studied by coupling them out from the metal surface, using a periodic structure of holes and slits, and measuring the spectrum of the light from these structures.

This research contributes to fundamental physics. Increasing the plasmon propagation length could lead to new applications.

1.2 Historical overview

R.H. Ritchie first predicted the existence of plasmons in 1957 and later, in 1968, he was also the first to measure them [1, 2]. In the spectrum of a metal reflection grating he found some wavelengths to be more reflective, showing up as peaks in the spectrum. This indicated that these wavelengths are resonant due to the periodicity of the grating. He was able to link some of these peaks to plasmon resonances.

A renewed interest in plasmons was sparked by the publication of T.W. Ebbesen's paper on the "extra-ordinary transmission of hole arrays" in 1998 [3]. He used a gold layer with a periodic array of nanoscale holes, similar to the gold layer used for our experiments. He was surprised that the amount of light transmitted by these small holes was higher than what could be expected from their size. To further investigate this phenomenon, called extraordinary optical transmission, the transmission spectrum was measured. The spectrum showed peaks and dips at frequencies related to the spacing of the holes, thus linking this effect to plasmons.

M.T. Hill (2007) made a nanolaser from a metallic coated nanocavity, demonstrating that losses of plasmon-like modes can be compensated by adding gain [5]. In this experiment the gain material is pumped electronically while in our system it was pumped optically.

J. A. Hutchison (2011) has added dye molecules, instead of a semi conductor,

as a gain material, to a metal hole array [6]. He found a peak in the transmission corresponding to the wavelength where the dye was expected to absorb and emit light. This phenomenon, called absorption-induced transparency, could again be linked to plasmons, since samples made out of a metal that does not support plasmons do not show this effect.

However, this paper did not study the propagation length of the plasmon. Furthermore, a disadvantage of dyes is that the spectral range at which they emit light is smaller than that of the gain medium used in our samples. With a broader spectral range more resonances become visible, making it easier to identify peaks caused by plasmon resonances.

Currently, plasmons are used in sensors that use surface enhanced Raman scattering to detect molecules absorbed on a metal surface [4]. Another application is in photovoltaic cells where the light absorption, and therefore the efficiency, is increased through the use of plasmons [7].

1.3 Outline

This master thesis is organised as follows:

- **Chapter 2 (Theory)** presents the theory of resonances in periodic structures. It continues by explaining how fluorescence results from pumping the gain layer with a laser and by predicting where gain can be expected.
- **Chapter 3 (Materials and methods)** describes all methods and settings used for measurements. Moreover, the set-ups and the sample design are discussed.
- **Chapter 4 (Sample characterisation)** starts with a characterisation of the optical properties of the metal structure based on the measured linear transmission. Next, the gain layer is investigated to check that it is not damaged by measuring its fluorescence.
- **Chapter 5 (Dispersion and propagation length)** answers the questions whether resonances can be found in the fluorescence spectrum and how a propagation length can be determined from a plasmon resonance. Finally,

the amount gain is influenced by changing the pump power and measurement angle. It is investigated whether the amount of gain increases the propagation length for plasmons and whether this gain can fully compensate for the losses.

- **Chapter 6 (Conclusion)** gives a summary of the results obtained.
- **Chapter 7 (Outlook)** lists possible design and measurement improvements.

Chapter 2

Theory

This chapter begins by explaining the origin of a resonance in the spectrum of a grating and how plasmon resonances can be identified. From the resonances the propagation length can be determined.

To understand the shape of the fluorescence spectrum, a description of the effects of pumping the gain layer with a laser is given. A mathematical model is given for fitting the fluorescence spectra and resonance peak for determination of the propagation length. Finally, the amount of gain and its dependences are discussed and theoretical estimates for the propagation length are made.

2.1 Resonances

The hole and slit array structures in the gold, act as a grating. There are two types of resonances that can be seen in the spectrum of a grating: plasmon resonances and Rayleigh anomalies. This section starts with explaining the origins of both resonances and ends with a discussion on how the resonances can be distinguished from each other.

2.1.1 Plasmon resonances

When a plasmon encounters a hole or a slit, it can couple out of the interface to a free-space photon. The signal measured by the spectrometer is a sum of all light emitted from the holes or slits. When the light coupled out by consecutive holes is in phase, there will be constructive interference. Thus a peak is found in the spectrum at the wavelength of the resonant light.

If the spacing between the slits or holes is the same as the effective wavelength of the plasmon, they will be coupled out resonantly. A small phase delay, caused

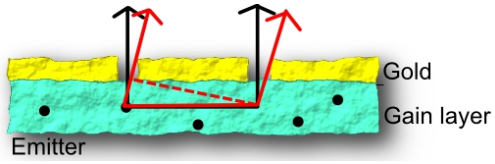

Figure 2.1: *Illustration that different wavelengths are coupled out resonantly under different angles since the path length changes with the angle.*

by a potential change in refractive index experienced at the holes, is neglected [8].

When measuring under an angle, the resonant wavelength will shift since there is an extra path length difference, as shown in figure 2.1. This extra path length is $\pm\sin(\theta)\cdot d$, where θ is the azimuthal angle and d is the spacing. Hence, the resonant wavelength can be calculated with:

$$\lambda = d\cdot(n_{eff}\pm\sin(\theta)) \tag{2.1}$$

Here λ is the wavelength and n_{eff} is the effective mode index.

For hole arrays more than one wavelength can be resonant. Not only are there plasmons that travel vertically or horizontally along the hole array in the (1,0) and (0,1) mode respectively, but there is also a (1,1) mode travelling diagonally. Since these modes have a different path length, the resonance conditions change. For the (1,1) mode the effective lattice spacing is $d/\sqrt{2}$, instead of d, as illustrated in figure 2.2.

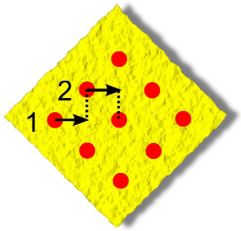

Figure 2.2: *A hole array with the (1,1) mode direction indicated by arrows. The path length needed for resonance is $d/\sqrt{(2)}$ so that the light emitted from row one is not only resonant with holes on the same row but also with the holes in row two.*

2.1.2 Rayleigh anomalies

A different type of resonance can be found in the spectrum of gratings or hole structures. This Rayleigh anomaly, also sometimes referred to as Wood anomaly or Rayleigh-Wood anomaly, occurs for both polarisation directions [9]. The study of these anomalies is an extensive field and goes beyond the scope of this thesis, therefore only the general concept will be explained.

Rayleigh anomalies are caused by the disappearing of diffraction orders, as illustrated in figure 2.3. When illuminating a grating with monochromatic light, the power of the light is spread over the different diffraction orders. However, for a resonant wavelength an particular order is transmitted parallel to the grating surface. When this order disappears into the surface, its the power moves to the other orders thus causing peaks and dips to appear in the optical spectrum.

(a) (b)

Figure 2.3: *These figures explain the origin of Rayleigh anomalies. In figure (a) we see light exiting the grating structure where a zero and first order are visible. When increasing the wavelength of the light, the order will be parallel to the grating surface and will then disappear. The power of this missing order is redistributed into the zero order, causing a Rayleigh anomaly to appear in the spectrum.*

Similar to the plasmon features, the centre wavelength of Rayleigh anomalies is angle dependent. The same resonance condition of formula (2.1) applies, but the Rayleigh anomalies have a different effective mode index.

2.1.3 Determining the propagation length

The propagation length of a plasmon can be found from the full width at half maximum (FWHM) of the resonance peak. The more periods a wave travels the better the resonance selection becomes, as illustrated in figure 2.4. Light with a

wavelength that is off resonance, will cause destructive interference from the light coupled out at the next opening. However, if light is only slightly of resonance it will have to travel more periods before it is in antiphase. Due to loss from travelling, this light will have a lower intensity and will not cancel out the original light. This leads to more signal in the spectrum around the resonance peak, increasing the FWHM.

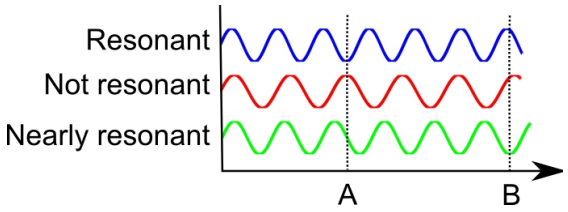

Figure 2.4: *Illustration explaining the FWHM decreases with propagation length. Three waves with different wavelengths are shown. The blue wave is presumed to be resonant with the structure. The red wave that is not resonant, interferes destructively after only a few periods at point A. The nearly resonant green wave only interferes destructively at B. At point B the amplitude of the wave will be smaller due to absorption. The remaining amplitude will no longer completely destructively interfere. Thus the green wave will still be visible, leading to a broadening of the resonance peak in the spectrum.*

Any excitation that decays exponentially has a Lorentzian shape resonance peak of the form:

$$I = I_{max} \cdot \frac{\frac{1}{2} \cdot \Delta\lambda}{(\lambda - \lambda_{\text{centre}})^2 + (\frac{1}{2} \cdot \Delta\lambda)^2} \tag{2.2}$$

Here I is the intensity, I_{max} a general prefactor, λ the wavelength and λ_{centre} the resonance wavelength. The FWHM, $\Delta\lambda$, of this resonance is related to the propagation length L (the 1/e intensity decay):

$$L = \frac{\lambda_{\text{centre}}^2}{2\pi \cdot \Delta\lambda \cdot n_{eff}} \tag{2.3}$$

In the experiment, this FWHM can be broader because of the wide range of angles collected by the imaging system. This angle range is expressed as the numerical aperture (NA) where NA $= \Delta \sin(\theta)$. The spread in θ in formula 2.1, increases with the NA and may lead to an increase in observed spectral width.

2.2 Fluorescence in semiconductors

The propagation length of plasmons is expected to increase due to the semiconductor layer. By pumping this layer with light, electron-hole pairs are created. These electron-hole pairs excite plasmons and create gain through the process of spontaneous and stimulated emission, respectively.

This section starts by explaining the physics of optical pumping of a semiconductor. Then a mathematical model is given for describing spontaneous and stimulated emission. This mathematical model is later used for fitting the data. Finally, the expected propagation length is calculated.

2.2.1 Pumping a semiconductor

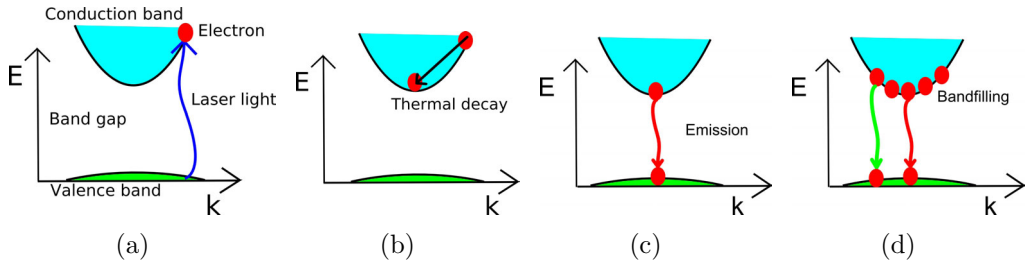

Figure 2.5: *The band structure for a semiconductor, showing valence band at the bottom, the band gap in-between and the conduction band at the top. When pumping the gain layer with a laser, electrons are excited, as seen in image (a). Due to fast thermal relaxation the electron moves to a lower energy state (b) and eventually emits light with a longer wavelength(c). When there are more electrons present, due to high pump power, band filling occurs. Since electrons cannot be in the same quantum state they can not thermally decay to the lowest energy level (d).*

In a semiconductor there are electron energy levels, called the band gap, that are absent. Light with a high enough energy can excite electrons from the valence band (lower energy levels) to the conduction band (higher energy levels), crossing the band gap. This is illustrated in figure 2.5(a). The absence of the electron in the valence band creates a vacancy, which is called a hole.

Through thermal decay, the electron moves to a lower energy (figure 2.5(b)) in the conduction band. Thermal decay is a very fast process (*ps* time scale) that is

assumed to happen practically instantly.

Through spontaneous emission of a photon, the electron can drop back to the valence band (figure 2.5(c)). The available energy can also be emitted as a plasmon. The wavelength can be calculated by using the relation $E = hc/\lambda_{vac}$ where E is energy, h is the plank constant and c the speed of light. This process happens on longer time scales than that of thermal decay.

As electrons are fermions, they cannot be in the same quantum state. When the pump laser power is increased, higher energy levels in the valence band thus become occupied. These electrons also relax through spontaneous emission, as shown in figure 2.5(d). This effect, called band filling, is observed in the spectrum as light with a wavelength shorter than the wavelength corresponding to the band gap.

A measure for the amount of band filling is the Fermi level or Fermi energy. This is the energy level that at which 50% of the states are occupied.

2.2.2 Mathematical model for fluorescence

The fluorescence spectrum is directly related to the energy density of the electrons and holes, since all electron-hole pairs have an equal probability for spontaneous emission. Thus a mathematical expression for the energy density of the electrons and holes is needed.

For the common parabolic band, the number of states available at an energy level ρ is proportional to the square root of the energy: $\rho \propto \sqrt{E}$. When at absolute zero temperature, the electrons will be distributed over the lowest possible energy levels.

The electron distribution over the energy levels, specified by the energy-dependent occupation $f(E)$, is described by Fermi-Dirac statistics: and is given by:

$$f = \frac{1}{e^{(E-E_f)/k_bT} + 1} \tag{2.4}$$

Where E_f is the Fermi level, T the temperature and k_b the Boltzman constant. In figure 2.6, the distribution is plotted for different temperatures.

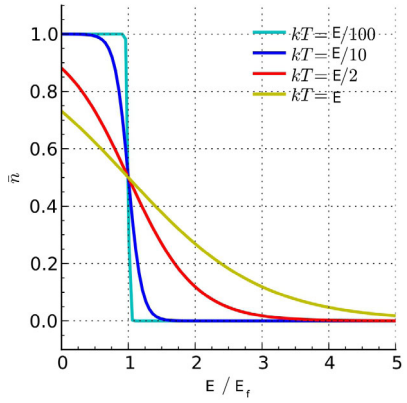

Figure 2.6: *The Fermi-Dirac distribution for four different temperatures. At low temperatures (blue) the lower energy levels are almost completely filled.*

By combining the density of states and the distributions of the electrons in the valence band (v) and electrons in the conduction band (c), the rate of spontaneous emission r_{sp} at a particular energy difference can be described as [10]:

$$r_{sp} = A \cdot \rho_v \cdot \rho_c \cdot f_c \cdot (1 - f_v) \tag{2.5}$$

Here A is the chance of spontaneous emission for a single electron hole pair. The number of states available in the valence band for the electrons to return to, is described by the $1 - f_v$ term.

For simplicity, the fluorescence caused by stimulated emission is not used for fitting. Furthermore, the Fermi-Dirac distribution and density of states of the valence band is not included since it can be approximated by a flat energy level. This is possible because the effective mass of the holes is larger than that of the electrons, therefore the prefactor of the square root, describing the density of states for holes, is an order in magnitude larger. This leads to:

$$r_{sp} \approx f(E)\sqrt{E - E_0} \tag{2.6}$$

In figure 2.7(a), the rate of spontaneous emission is shown as function of the energy. The rate of stimulated emission r_{st}, which is also plotted, is discussed in the next section. The high energy tail of spontaneous emission rate reflects the Fermi-Dirac distribution shape.

2.2.3 Mathematical model for stimulated emission

A second process, called stimulated emission, also causes fluorescence. Light created through spontaneous emission may stimulate electron-hole pairs to emit an extra photon with the same phase. Likewise, if a plasmon encounters an electron-hole pair, an extra plasmon can be created. It are these extra plasmons that compensate for absorption and lead to an increase in the propagation length. The amount of stimulated emission is proportional the gain coefficient. The rate of stimulated emission (r_{st}) is given by [10]:

$$r_{st} = A \cdot \rho_c \cdot \rho_v \cdot (f_c - f_v) \tag{2.7}$$

In figure 2.7(a) the rate of stimulated emission is plotted. The amount of gain changes with energy (thus also wavelength) and a maximum gain is found at E_m in the figure, where the stimulated emission peaks.

The amount of gain is related to the electron density, and increases with pump power. In figure 2.7(b) the gain factor for GaAs is plotted as function of energy at different electron densities. At higher densities gain is generated, while at low electron densities there is only a decrease in the amount of loss.

2.2.4 Theoretical propagation length

The propagation length can be estimated from the momentum (k) of the plasmon mode and the dielectric constants (ϵ) of the gold and InGaAs layer. The momentum of the plasmon mode can be calculated with [11]:

$$k_{plasmon} = k_0 \sqrt{\frac{\epsilon_{Au} \cdot \epsilon_{InGaAs}}{\epsilon_{Au} + \epsilon_{InGaAs}}} \tag{2.8}$$

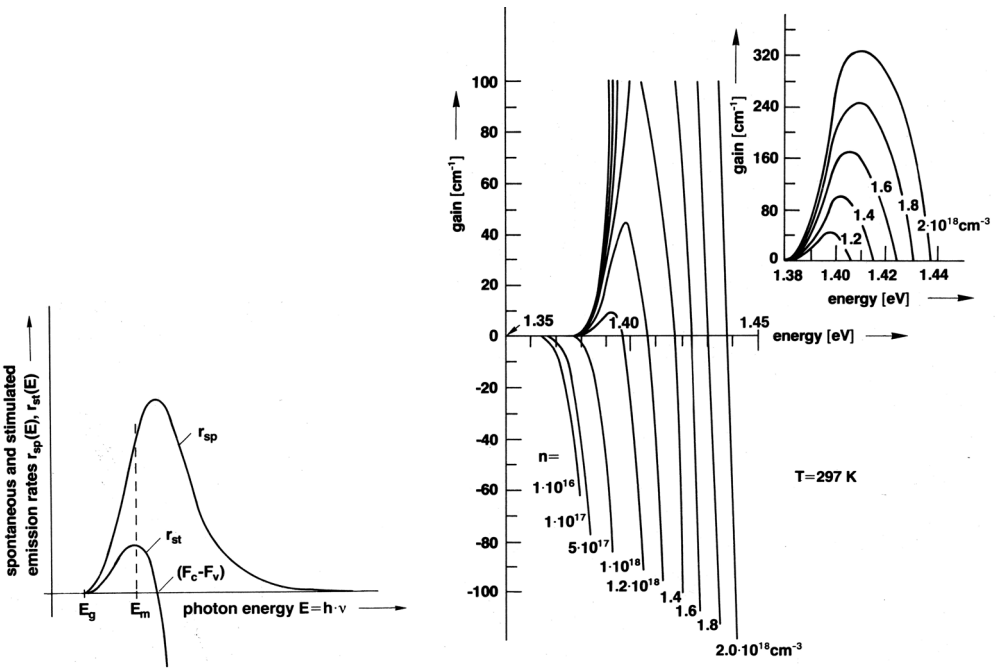

(a) (b)

Figure 2.7: *Figure (a) shows the spontaneous (r_{sp}) and stimulated (r_{st}) emission rates as function of photon energy. Figure (b) shows the calculated stimulated gain coefficient as function of photon energy for GaAs at different electron densities (n). Figures are taken from K. Petermann [10].*

The imaginary part of the momentum determines the amount of absorption. The propagation length can be found using:

$$L = \lambda_0/(4\pi \cdot n_{imaginary}) \tag{2.9}$$

The optical properties of the InGaAs layer change with wavelength and amount of pumping. The imaginary part of the effective mode index increases and can even become positive with pumping. The propagation length is calculated for three different amounts of pumping for a wavelength of 1500 nm. For an unpumped gain layer, a propagation length of 0.4 μm is expected [12, 13]. A gain layer pumped to transparency, i.e. it has no absorption by setting the imaginary part of the dielectric constant equal to zero, has a propagation length of 3 μm. Finally a maximally pumped gain layer can potentially cause infinite propagation length. These estimates do not include losses caused by hole or slit structures.

Chapter 3

Materials and methods

This chapter begins with a description of the calibration and the measurement technique of the spectrometer, used to measure the transmission of the sample and the fluorescence from the gain material. It continues with the respective set-ups and concludes with the sample design. The measurement settings described in this section are used for all the results discussed in the next chapters, unless explicitly stated otherwise.

3.1 Spectrometer calibration and operation

The infra-red camera (Xenics Xeva-642) attached to the output port of the spectrometer (HR 320 Monochromator Jobin Yvon) records all the transmission and fluorescence spectra. This section starts by explaining the camera settings, its non linearity correction, and its computer controlled read out. Afterwards the spectrometer operation, calibration and wavelength sensitivity are discussed.

3.1.1 Camera calibration

The camera is controlled with software from the manufacturer typically using the low gain mode and the 20 ms calibration pack standard settings. Small signals need to be measured with longer integration times. However, the software limits the integration time to 100 ms. To overcome this problem multiple frames are used with the frame integration option.

For the experiments it is important that the camera signal is linear with the intensity. To test the linearity, a reference signal is sent into the spectrometer. The intensity of the reference signal is controlled by two polarisers and is determined from the difference in angle between the polarisers. For a linear camera the

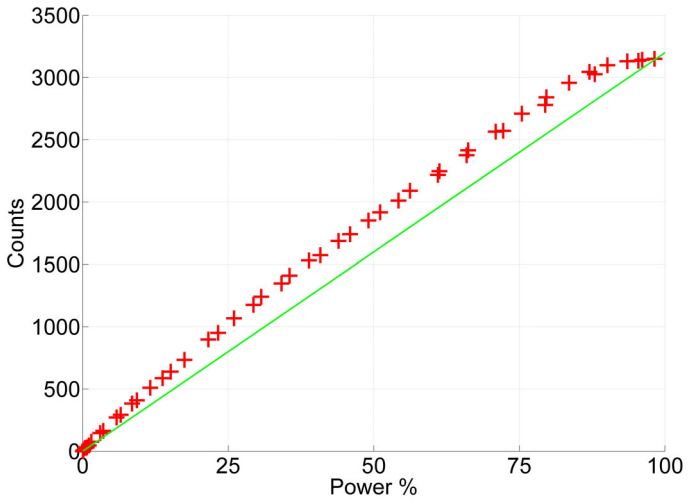

Figure 3.1: *The number of counts measured by the camera as function of percentage of power, for 422 frames with an integration time of 20 ms. The number of counts is not linear with the signal power.*

intensity should be proportional to the number of counts measured by the camera.

Measuring with different integration times and different numbers of frames, changes the non linear behaviour, thus fixed integration time and frame settings are used for all measurements. The non linearity for the fixed integration time of 20 ms with 422 frames is shown in figure 3.1. The measured curve is fitted with a polynomial. This polynomial is used to correct the intensity.

Since the non-linear response of the camera changes with the integration time, neutral density filters (NE, Thorlabs) are used to prevent high signals from saturating the camera. The transmission of these filters has been measured and the result is used to correct the measured spectra.

The data from unilluminated parts of the image is used for background subtraction. Three rows of pixels, that measure the centre of the pump spot, are averaged for the data in the final spectrum.

3.1.2 Spectrometer calibration

The spectrometer has a grating (Horiba Jobin Yvon) with a grove density of 150 mm^{-1} that is blazed at 1200 nm. In a grating spectrometer, the reflection angle depends on wavelength such that light of a certain wavelength will only fall on pixels of the camera at the corresponding horizontal position.

The camera has 320 pixels in the horizontal direction, limiting the range in wavelengths that can be measured from a single image. To increase this range the angle of the spectrometer grating is changed. This angle determines which wavelength falls on the centre of the camera. Images taken with different grating angles are stitched together to measure a spectrum from 950 nm to 1650 nm.

The entrance slit of the spectrometer codetermines the spectral resolution and is never wider than 0.1 mm. The spectral resolution, determined from the FWHM of a monochromatic laser signal, is 3 nm.

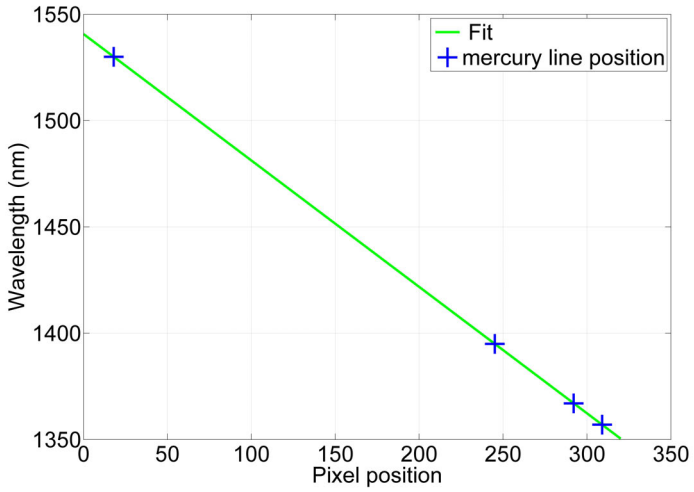

Figure 3.2: *The position of the mercury lines on the spectrometer camera. From the fit it is found that one pixel corresponds to 0.595 nm.*

Pixel position and wavelength were calibrated using two different references. The first was an NdYAG-laser of 1064nm and the second reference was a series known infra-red lines of mercury [24]. In figure 3.2 the measurements show that

the pixel position on the camera is linearly related to the wavelength. By fitting the data with a line, it is concluded that one pixel corresponds to a wavelength width of 0.595 nm.

The spectrometer has a different sensitivity for different wavelengths and polarisations. To compensate for this effect, a known spectrum of a calibration lamp is measured. The wavelength sensitivity of the spectrometer is found by dividing the measured spectrum by the expected spectrum. The result, shown in figure 3.3, is used to correct all other spectra.

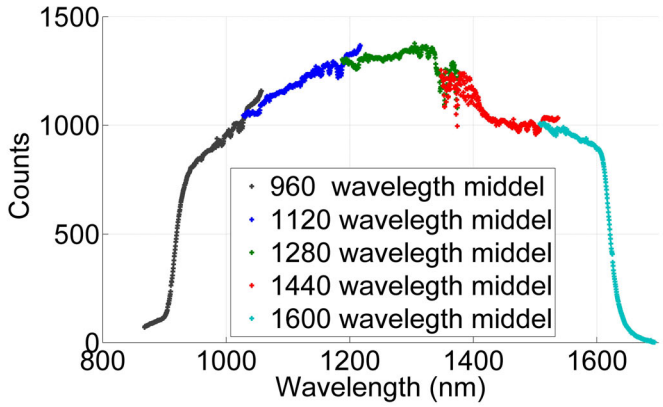

Figure 3.3: *The measured spectrum of the calibration lamp divided by the known spectrum of the calibration lamp. Every colour corresponds to a single image. This data is used to correct for the wavelength dependence of the spectrometer camera combination.*

3.2 Set-up

Next the two set-ups that use the same spectrometer is described. All lenses (Thorlabs) are achromatic and have antireflection coatings for 1050 nm to 1620 nm. All mirrors are silver and have an average reflection of more than 97.5% for our wavelength range. The first set-up measures the linear transmission of the sample; The second set-up measures the fluorescence from the optically pumped gain layer.

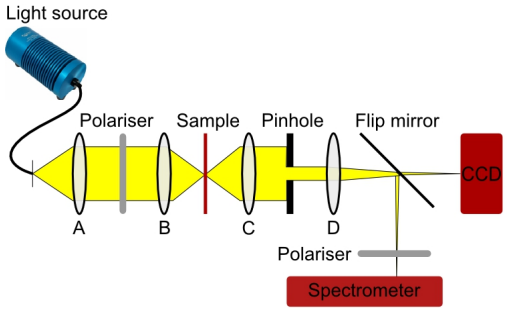

Figure 3.4: *Schematic view of the set-up for transmission measurements.*

3.2.1 Linear transmission set-up

The set-up used for linear transmission measurements is shown in figure 3.4. Light from a halogen lamp (HL-2000, Ocean optics) is focused through lenses A and B on the sample. Then the sample is imaged by lenses C and D onto the CCD camera (DMK ,The Imaging Source) for general alignment. By inserting the flip mirror, the light transmitted through the sample, is sent to the spectrometer. Lenses A, B, C and D have a focus of 5 cm, 5 cm, 10 cm and 30 cm respectively.

The pinhole in the Fourier plane is used to limit the NA. An NA of 0.04 is used in order to resolve spectral features, while keeping enough signal to accurately measure the spectrum. The polarisers are aligned parallel to each other and when measuring the slit array measurements, they are aligned perpendicularly to the direction of the slits.

The transmission is found by dividing the spectrum of the light that passes through the sample by the spectrum of the halogen lamp recorded without the sample.

3.2.2 Fluorescence set-up

Figure 3.5 shows a schematic image of the fluorescence set-up. The set-up can be split into two parts: A pump beam arm, that starts with the laser and ends at the sample, and an imaging arm that stretches between the sample and the spectrometer of CCD. The lenses A, B, C and D have a focus of 5 cm, 3 cm, 20 cm and 10 cm respectively.

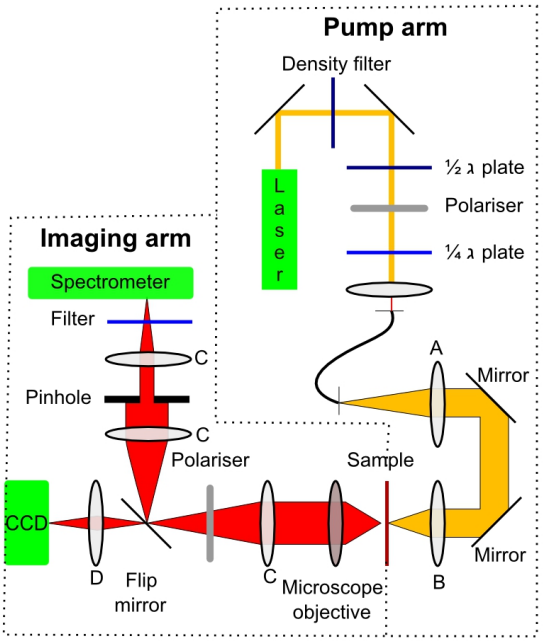

Figure 3.5: *Schematic view of the set-up for fluorescence measurements.*

This section starts by looking at the pump beam arm. The laser (NdYAG CL 1064-500, Chrystalaser) has a wavelength of 1064 nm and a power of 500 mW. To control the laser power, a density filter wheel and a half lambda plate with polariser are used. To increase the output power stability, a quarter lambda plate is used to minimalise back reflection. The laser light is coupled into a single-mode fibre with a coupling efficiency of 52%, resulting in a maximum power of 260 mW. At the other end of the fibre, the pump light is collimated with a moveable lens. Moving this lens controls the pump spot size. Finally the laser light is focused onto the sample.

In the imaging arm the sample the combination of a long working distance microscope objective (M Plan Apo NIR, Mitutoyo) with of an NA of 0.40 and a tube lens C make an intermediate image in a plane near the flip mirror. For general alignment this flip mirror is removed and the intermediate plane is imaged on a CCD camera (DMK ,The Imaging Source). In order to measure a spectrum, the flip mirror sends the light through two more lenses, which image the intermediate plane onto the entrance slit of the spectrometer. Before the light enters the spectrometer,

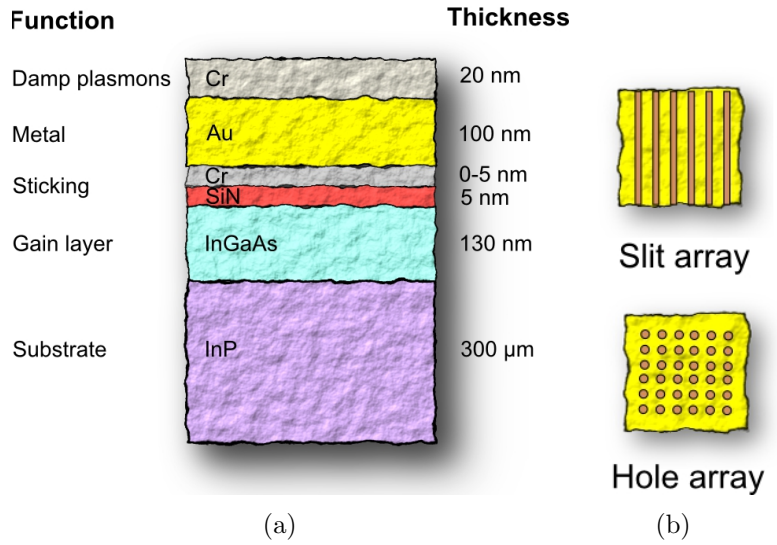

Figure 3.6: *Schematic image of the (a) cut-through of the sample and (b) the structures in the gold and chromium surface.*

the pump light is filtered out, using a longpass filter (FEL 1100, Thorlabs).

The polariser in the imaging arm can be used to measure the polarisation dependence of the fluorescence. The sketched pinhole is located in the Fourier plane and can be used to change the NA and control the measurement angle. Neutral density filters are placed behind the microscope objective to control the intensity.

The sample is put in a custom-made flow cryostat (Cryovac) that has anti-reflection coated windows. This cryostat can be cooled using either liquid nitrogen or helium. A built-in thermometer and heater are used to monitor and control the sample temperature. However, note that the temperature probe is located at a distance from the sample holder and does not measure the temperature of the sample at the pump spot.

The fluorescence is generally measured at a fixed temperature of 77 K, using liquid nitrogen as cooling liquid. The standard pump spot size is 10 μm.

3.3 Sample design

In figure 3.6 (a) a schematic image of the cross section of a sample is shown. The sample is grown on a InP substrate of 300 μm thickness. Covering it, there is a 130 nm thick layer of $In_{0.53}Ga_{0.47}As$, a gain material.

To stop electrons from being drawn away from the InGaAs layer into the gold (Au), an isolation layer of SiN of 5 nm is put on top. For adhesion of the gold layer, a thin layer of chromium (Cr) is used. The thickness of this chromium layer cannot be accurately controlled but is 0-5 nm. Since only the plasmons travelling through the InGaAs are of interest, plasmons forming on the other side of the gold layer are prevented by depositing a 20 nm thick layer of chromium. This chromium absorbs any plasmons here.

A periodic structure of 50 x 50 μm^2, is made in the gold and chromium layers. The two types of structures, slit and hole arrays, are shown in figure 3.6 (b). The hole and slit diameter is 100$\pm$20 nm. Samples with spacings ranging from 300 nm to 800 nm with increments of 100 nm have been made.

Chapter 4

Sample characterisation

The goal of this chapter is to characterise the sample, and to compare the results with theory or numerical simulations. Optical resonances of the hole and slit arrays are studied through measurements and simulations of the linear transmission. This helps to identify Rayleigh and plasmon resonances.

Properties of the gain material (InGaAs) are characterised by pumping the layer with a laser and by measuring the resulting fluorescence. These fluorescence measurements contain information on the amount of band filling, sample temperature and electron-hole pair diffusion.

4.1 Transmission measurements and simulations

The linear transmission is the percentage of light that passes through the sample. This transmission is wavelength and polarisation dependent. Resonant wavelengths can show up as maxima in these measurements. A detailed description of how the transmission is measured can be found in chapter 3.

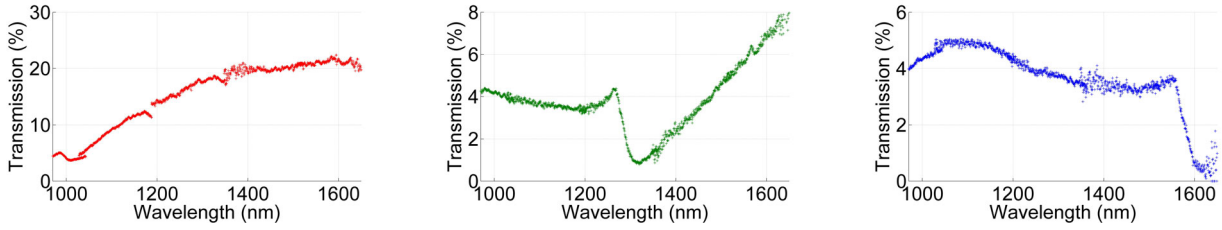

(a) *300 nm slit array* (b) *400 nm slit array* (c) *500 nm slit array*

Figure 4.1: *The transmission spectra of samples with a slit array. In the samples with a larger spacing transmission maxima move to larger wavelengths. The maxima are seen at approximately 990 nm, 1265 nm and 1550 nm.*

In figure 4.1 the transmission measurements of the slit array samples are shown. The transmission generally increases with wavelength, but at some wavelengths a local maximum followed by a minimum is seen. These maxima are seen at approximately 990 nm, 1265 nm, 1550 nm for the 300 nm, 400 nm and 500 nm spacing, respectively.

As explained in section 2.1, the resonant wavelength can be used to calculate the effective index of the mode. For each of the slit arrays an effective mode index of 3.2±0.1 is calculated. Quite surprisingly, this value is comparable to the index of of the InP substrate. Since the plasmon is expected to be in the InGaAs layer, which has a refractive index of 3.6, the low mode index implies that these maxima in the transmission are not caused by a plasmon resonance, but rather by a Rayleigh anomaly.

Using Rsoft DiffractMOD software, the transmission is simulated numerically. See figure 4.2 for the results. For these simulations the chromium layer under the gold is assumed to be 2 nm thick. The amount of absorption is determined by the imaginary part of the dielectric constant of the InGaAs, which was set to 0.2.

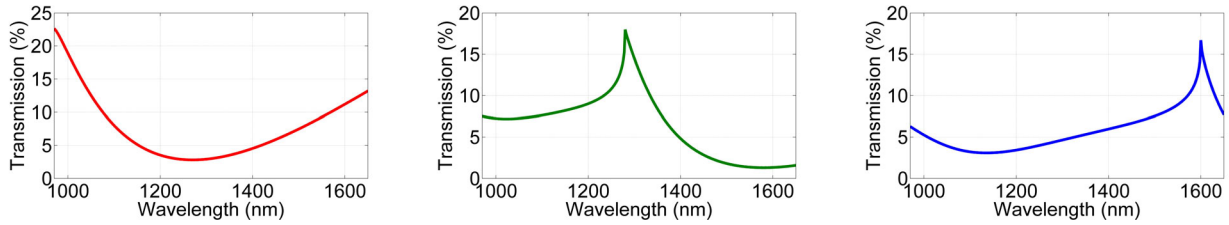

(a) *300 nm slit array* (b) *400 nm slit array* (c) *500 nm slit array*

Figure 4.2: *Simulation of the transmission spectra of the slit arrays. The simulations were made for a sample with a 2 nm chromium layer. The maxima are exactly at the Rayleigh wavelength*

Both the percentage of transmission and the general shape of the simulated transmission are comparable to the measurements. Interestingly, the maxima are at exactly the Rayleigh wavelength for InP, indicating that the features seen are Rayleigh anomalies. Furthermore, changing the absorption of the InGaAs layer in the simulation has little effect on the transmission.

Maxima that can be attributed to plasmon resonances are not seen. This may

be due to the high amount of plasmon losses that result from the slit structure. These structures may cause all the plasmons to couple out.

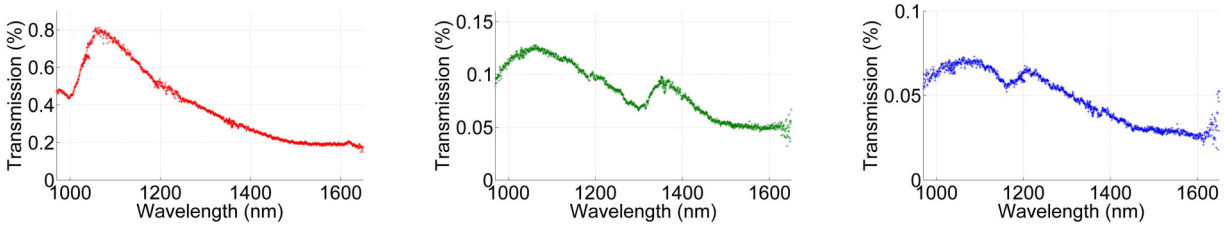

(a) *300 nm hole array* (b) *400 nm hole array* (c) *500 nm hole array*

Figure 4.3: *The transmission spectra of hole array samples. The general transmission is more than an order in magnitude lower than the slit array transmission. The maxima are seen at approximately 1070 nm, 1360 nm and 1215 nm.*

In figure 4.3 the transmission of the hole arrays is shown. The typical transmission factor is more than an order of magnitude smaller than that of the slits. A large difference is expected since the hole samples have a smaller perforated area in the gold surface, thus allowing less light to pass through.

Maxima are seen in the hole array transmission spectra at 1070 nm, 1360 nm, 1215 nm for the 300 nm, 400 nm and 500 nm spacing, respectively. The minima are now found at shorter wavelengths than the maxima, whereas the slit arrays showed minima at longer wavelengths. The maxima seen in the 300 nm and 400 nm hole arrays are at longer wavelengths than the maxima of the slit array with the same spacing.

To help interpret these results, the simulations of the hole arrays are shown in figure 4.4. There are two shapes that can be seen in these simulations.

The first shape is a very small sharp peak that can only be seen clearly when zooming in at 1600 nm for the 500 nm spacing. This small peak is also visible at 1280 nm for the 400 nm spacing, however it's position coincides with the maximum of the second shape. These peaks are at the Rayleigh wavelength indicating that they convey similar physics as the Rayleigh anomalies that were previously observed with the slit arrays.

The second shape is the clearly visible minimum followed by a maximum, features that are also visible in the measurements. This shape is not a sharp point,

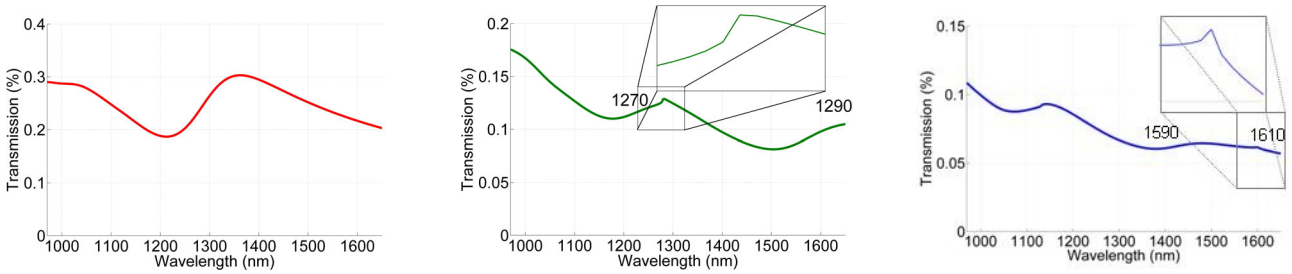

(a) *300 nm of hole array* (b) *400 nm of hole array* (c) *500 nm of hole array*

Figure 4.4: *Simulation of the transmission spectra of the hole arrays. The simulations were made for a sample with a 2 nm chromium layer. A small sharp peak can be seen at 1280 nm for the 400 nm spacing or at 1600 nm for the 500 nm spacing. These are at the Rayleigh wavelength. Other maxima can also be seen at 1360 nm, 1290 nm, 1150 nm for the 300 nm, 400 nm and 500 nm spacing respectively.*

like the Rayleigh anomaly peaks, but a smooth peak. Furthermore, the minima are at shorter wavelengths than the maxima, instead of at longer wavelengths as seen with the Rayleigh anomalies. This difference in shape indicates that this is a plasmon resonance.

The maximum seen at 1300 nm in the 400 nm sample is assigned to the (1,1) mode that runs diagonally across the hole array, since another peak is forming near 1600 nm corresponding to the (1,0) mode. The same argument can be used to identify the maximum seen in the 500 nm sample at 1150 nm as a (1,1) mode.

To further investigate whether these maxima are plasmon resonances, the simulations were repeated with a smaller imaginary part of the index for the InGaAs layer, thus decreasing the plasmon absorption. The larger features, identified as plasmon resonance, become more prominent. This supports the hypothesis that it is a plasmon resonance. Furthermore, the small sharp Rayleigh peaks remain very similar to those seen in the simulation with absorption.

Another indication that this larger feature is a plasmon resonance, is the effective mode index. From the position of the maxima of the simulations an effective mode index of 4.5, 4.6 and 4.6 is found for the the 300 nm, 400 nm, 500 nm spacings respectively. The value of the index is high compared to the refractive index (3.6) of InGaAs, but it could be realistic. When calculating the effective index for a plasmon, including the gold layer, an index of 3.9 is expected. Literature shows

a 5% increase in index due to the holes in a sample for the (1,0) modes [20]. The effect of the holes is expected to be even larger for (1,1) modes.

For the 300 nm spacing hole sample, a transmission peak at 1350 nm is predicted from simulations. However this peak does not appear in the measurements. The absence of this plasmon resonance is not yet understood.

4.2 Fluorescence

The spectrum of the fluorescence is studied to investigate whether the InGaAs layer works as expected. A spectrum similar to figure 2.7(a), as explained in section 2.2, is expected. When increasing pump power band filling should be visible.

Next the fluorescence spectrum of the samples with and without periodic structures in the gold surface are compared, to see whether they cause resonances. A detailed description of how these spectra are measured is found in chapter 3.

In figure 4.5(a) the spectra of the InGaAs layer without a structure in the gold layer, are shown using different pump powers. The shape of the fluorescence spectrum is similar to the shape expected from the theory discussed in section 2.2. When increasing the pump power, the fluorescence moves to shorter wavelengths, which is the band filling effect.

The band gap wavelength increases with pump power. The movement of the band gap indicates an increase in temperature. This will be discussed in more detail in section 4.4.

Another intriguing feature is the continuous increase in the number of counts at large wavelengths close to the band gap. Due to the fermion nature of electrons, only a limited amount of electrons can be put into an energy level, thus limiting the amount of fluorescence that can be emitted at a particular wavelength. These levels should be more quickly filled at large wavelengths than at shorter wavelengths.

The observed increase might be explained by the changing band gap caused by the increase in pump power. This results in a shift of the energy levels, causing an increase in the number of possible states for a fixed energy. An increase can also

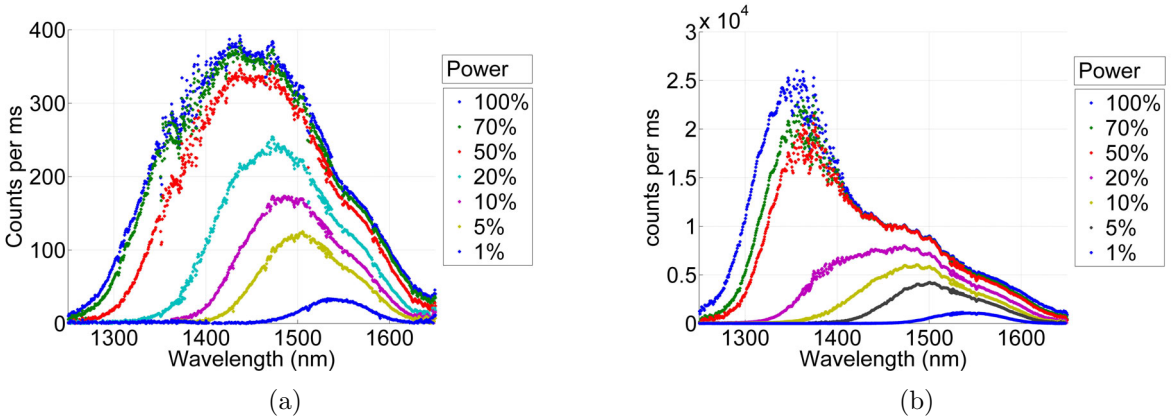

(a) (b)

Figure 4.5: *The spectrum of the fluorescence with different pump powers of (a) gold with no structure, (b) slit array with 400 nm spacing. The spectrum of the slit array shows a peak at 1380 nm. 100% power corresponds to 260 mW.*

be expected for the stimulated emission.

Figure 4.5(b) shows the fluorescence spectra of the sample with a 400 nm spacing slit array in the gold layer. At low powers it is similar to the fluorescence seen with the sample without any structure. At high powers an intriguing peak appears at 1380 nm. This shows that the structures can influence the fluorescence of the sample.

4.3 Fitting

By fitting the spectra, using the model as discussed in section 2.2, values are found for the band gap, the Fermi level and the temperature. The spectra without resonances are fitted with equation 2.6.

The spectra with peaks from resonances, are fitted using the same fluorescence equation, but supplemented with an extra Lorentzian function, as shown in equation 2.2, to fit the peak. This extra Lorentzian allows values to be found for the propagation length and position of the resonant mode.

In figure 4.6 the fluorescence of the 400 nm spacing slit array, measured using 260 mW pump power, is compared with the fit. The resulting fit parameters and errors can be found in table 4.1.

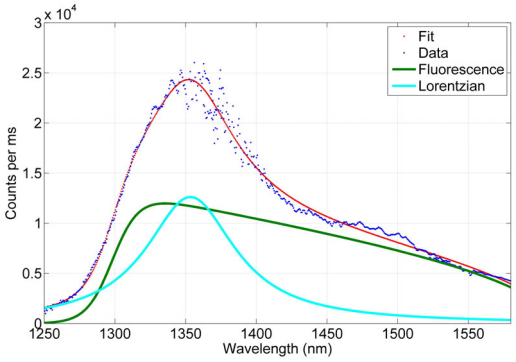

Figure 4.6: *The fluorescence of the 400 nm spacing with slit array at 260 mW fitted with the fluorescence model and a Lorentzian. The red curve is the total fit. The green curve is the part caused by the fluorescence and the blue curve is the Lorentzian.*

Band gap(nm)	Fermi energy(nm)	FWHM(nm)	peak position(nm)	Temperature(K)
1608±4	1299±1	75±1	1353±1	79±6

Table 4.1: *The fit parameters found from figure 4.6.*

The values found using the fit are plausible. If there was a sharp drop at the band gap it would be expected around 1610 nm. The gamma gives a FWHM of 75 nm and the centre position of the peak is near 1350 nm. The temperature is discussed in the next section.

The error in the fit is surprisingly small. It is clearly underestimated due to the fact that this error only takes the statistical variations into account, but not systematic errors. For example, the variations that are caused by the limitations of the model are not included in the error estimation. Examples of such a variation are the increase in fluorescence caused by stimulated emission and the impurities of the InGaAs layer.

To minimise errors, the fitting range has been changed to avoid area's where the data differs from our model, such as the area near the band gap. The error from the stimulated emission does not seem to affect the fit.

In the following sections this fitting procedure is used to help determine the sample temperature, the centre of the peaks and the propagation length.

4.4 Sample temperature measurement

Temperature control is important since the pump laser heats the sample and may cause damage. Additionally, temperature changes the physical properties of the InGaAs layer. An example is the band gap increase with temperature. This has already been seen in figure 4.5(a) where the fluorescence of the InGaAs was measured with different pump powers, thus different temperatures.

The Fermi-Dirac distribution that partly determines the electron density and also the amount of gain, is temperature dependent. Due to this effect more gain is expected for lower temperatures, thus increased plasmon propagation length. Electron diffusion, see section 4.5, also decreases with temperature. Less electron diffusion means that electrons will remain within the pump spot which will lead to more gain.

An extra motivation for keeping the sample cold is that at low temperatures the heat conduction in the sample will improve. The thermal conductivity increases one order in magnitude, when cooling from 100 K to 11 K [21].

There are three methods to measure the temperature of the sample. The internal thermometer, the movement of the band gap and fitting the fluorescence.

The thermometer is located far from the pump spot and does not measure the local temperature of the pumped InGaAs layer. When using a high pump power, the local temperature may greatly increase, while only a small increase in temperature is measured at the thermometer. This indicates that the thermometer only gives reliable results for low pump powers.

The band gap change with temperature can also be used as a temperature indicator. The band gap determines the maximum wavelength of the fluorescence. The change in the band gap can be seen in figure 4.7(a). The featureless spectrum of the 300 nm spacing slit array is measured with a low pump power of 2 mW at different temperatures. These temperatures are measured by the cryostat thermometer.

The band gap does not change between 4 K and 80 K. However, the band gap

for 160 K (purple) and 240 K (green) moves to larger wavelengths.

The band gap is determined by using the fitting procedure as described in section 4.3. The resulting band gap as function of the temperature is plotted in figure 4.7(b). The movement of the band gap increases almost quadratically with the temperature as expected from Varshni empirical law [16]. The literature predicts the band gap of InGaAs at 1680 nm at 300 K and 1510 nm at 4 K [14].

The difference between the measured band gap and the literature could be due to the InP layer causing strain. At the interface between two layers with different thermal expansion coefficient, mechanical stress and strain will build up when changing temperature. This tension leads to a change in the band gap. The InP layer differs 20% in thermal expansion coefficient, compared to that of the InGaAs [18, 19].

The exact ratio of In to Ga also determines the band gap. If the ratio changes from 47/53 to 48/52, a 5% change in band gap is already expected [17].

Figure 4.7(a) shows that the overall amount of fluorescence also changes with the temperature. This is unexpected as the same amount of fluorescence would be expected, since the pump power is not changed during the measurements. This effect is not yet understood but might be caused by Fabry-Perot interference of the pump laser with the substrate.

The third way to determine the temperature is by fitting the measured spectra with the fluorescence model, as explained in section 4.3. To get a better indication of the temperature only the data at the shorter wavelengths is used. In this part of the curve the Fermi-Dirac distribution term, which contains the temperature information, is dominant. Higher temperature produce smoother spectra.

In figure 4.8 the temperature determined from the fit of the spectra in 4.7(a), is plotted against the temperature measured by the cryostat thermometer. This comparison is acceptable, however for temperatures above 50 K, the fit gives a lower temperature than the thermometer on the cryostat. Furthermore, the fitted temperature does not drop below 20 K even when the sample is cooled to 4 K. This is a significant difference that could be due to the decrease in thermal conductivity

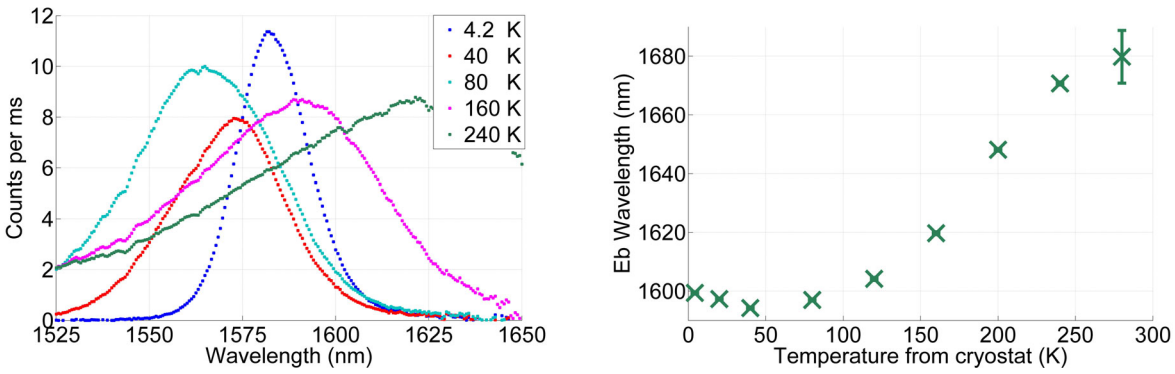

(a) (b)

Figure 4.7: *Figure (a) shows the fluorescence of the 300 nm-spacing slit array at different temperatures with modest 2 mW pump power. Upon heating, the band gap moves to larger wavelengths. In (b) the temperature measured by the cryostat thermometer is plotted against the band gap found from the fit.*

below 20 K [21].

The temperature of the sample increases significantly when using 260 mW pump power. Although the internal thermometer measures only an increases to 4.8 K when cooling the cryostat to 4.2 K, the sample temperature rises to 160 K, according to the fitted spectra, or to 200 K, when comparing the position of the band gap. Thus using more pump power, may not improve the amount of gain. Using a larger pump spot or less power, should be considered.

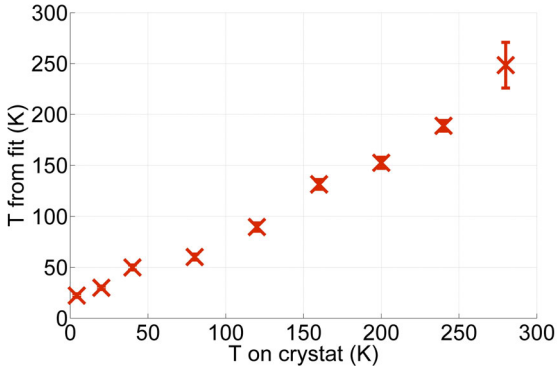

Figure 4.8: *The temperature determined from the fit of the spectra in 4.7(a) plotted against the temperature measured by the cryostat. The temperature from the fit and the temperature from the cryostat are in reasonable agreement.*

4.5 Carrier diffusion

The electron-hole pairs, made by pumping the InGaAs, may diffuse away from the pump spot. This loss of pairs from the spot is inefficient use of pump power. The loss and what can be done to prevent it, is discussed in this section.

The diffusion length depends on the concentration of electrons, the temperature, the lifetime (τ) and the electron mobility (μ):

$$l_{diffusion} = \sqrt{(\mu k_b T/e)\tau} \tag{4.1}$$

The electron mobility is also temperature dependent and has a maximum at around 80 K and decreases one order in magnitude when cooled to 20 K or heated to 180 K [22]. The hole mobility is about an order of magnitude lower due to their larger effective mass.

The hole mobility has been observed to decrease by a similar order of magnitude upon heating [23]. Data for temperatures lower than 80 K have not been found.

The electron diffusion can be studied comparing the width of the pump spot and the fluorescence spot. Diffusion causes the fluorescence spot to be wider than the pump spot. By cooling the sample the diffusion should decrease.

For the experiment a pump power of 2 mW was used. The number of counts are normalised to the maximum so the width can be compared. The pump spot is filtered out using an interference filter.

Figure 4.9 shows the observed spatial cross sections. The diffusive spot is always larger than the laser spot (red). Between the 20 K (blue) and 80 K (green) cross sections there is no significant difference in width. However, an increase in width is seen at 160 K. This confirms that cooling decreases the electron mobility.

A second method to visualise the diffusion length is by looking at the images taken with a spectrometer. Different wavelengths fall on different pixels in the x-direction, however the y-direction still contains spatial information. A larger diffusive spot will result in a wider cross section in the y-direction.

A few cross sections at different wavelengths (x-position) of the spectrum of the InGaAs layer, measured through the gold using full pump power at 77 K, are shown in figure 4.10(a). The counts are normalised to the maximum.

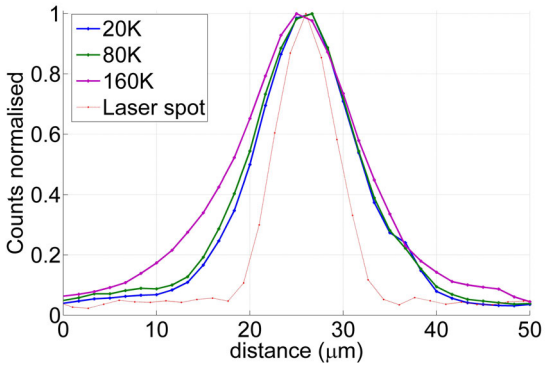

Figure 4.9: *A cross section of the diffusive spot, imaged in the zero order of the spectrometer, using a pump power of 2 mW power on surface with gold. A widening of the diffusive spot with temperature is seen.*

The image shows that larger wavelengths have a wider cross section. The diffusing electrons experience a change in the energy density distribution. The reason for this is as follows: when an electron moves out of the pump spot, it encounters less electrons, thus more free lower energy levels. Due to fast thermal energy dissipation the high energy electrons drop to lower energy, thus emitting light with a larger wavelength.

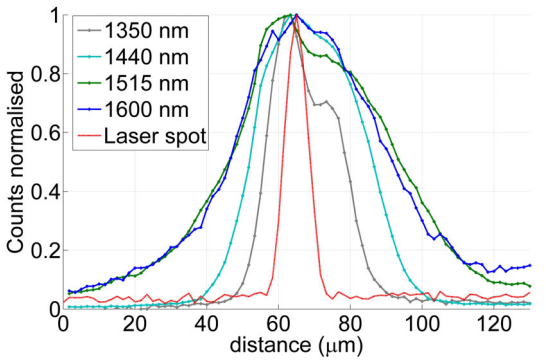

(a)

Figure 4.10: *Vertical cross section at different wavelengths of the fluorescence spectrum, measured through unstructured gold, using full pump power. At larger wavelengths the diffusive spot widens.*

Chapter 5

Dispersion and propagation length

From the linear transmission it has been shown that there are Rayleigh anomalies and plasmon resonances in the samples. In chapter 4 the peaks in the fluorescence measurements has been seen. In this section, these peaks are further studied in view of their potential for lossless plasmonics.

The angle dependence of the fluorescence will be used to accurately determine the effective mode index. This helps the identification of Rayleigh and plasmon resonances. Next the influence of the gain on the propagation length is examined by changing the measurement angle and pump power. The chapter concludes by observing the polarisation dependence of the resonances, making it possible to distinguish the propagation direction of the modes.

5.1 Angle selection

Due to the grating structures, a change in the NA or the measurement angle will influence the measured fluorescence spectrum. The centre resonant wavelength can be accurately determined by measuring spectra under different angles.

By decreasing the NA by closing the pinhole in the Fourier plane, the range of angles collected in the imaging system is narrowed. Figure 5.1(a) shows the spectrum of the 500 nm spacing slit array, measured with different NA. These measurements were made using 260 mW pump power and the standard measurement settings as explained in chapter 3. To compare the spectra, the number of counts are normalised to the maximum of the peak. As the NA is decreased, the

FWHM of the peak also becomes smaller.

To study this effect in a more quantitative manner, the fitting method described in section 4.3 is used to determine FWHM of the feature. In figure 5.1(b) the FWHM is plotted as a function of the NA. The FWHM decreases linearly with the NA until it remains constant for an NA smaller than 0.07.

Increasing the pump spot size from 10 μm to 20 μm diameter, while measuring the spectrum with an NA of 0.05, does not effect the FWHM. This indicates that the propagation length is only bounded by the losses.

Measuring with an NA smaller than 0.05 results in two experimental problems. Limiting the NA reduces both the amount of signal and the spatial resolution. With an NA smaller than 0.05 the centre of the pump spot can not be clearly resolved. This causes the intensity of the fluorescence from the centre of the pump spot to be averaged with the fluorescence from the edges of the spot, resulting in a lower peak intensity. Such spectral smoothing can lead to underestimation of the propagation length.

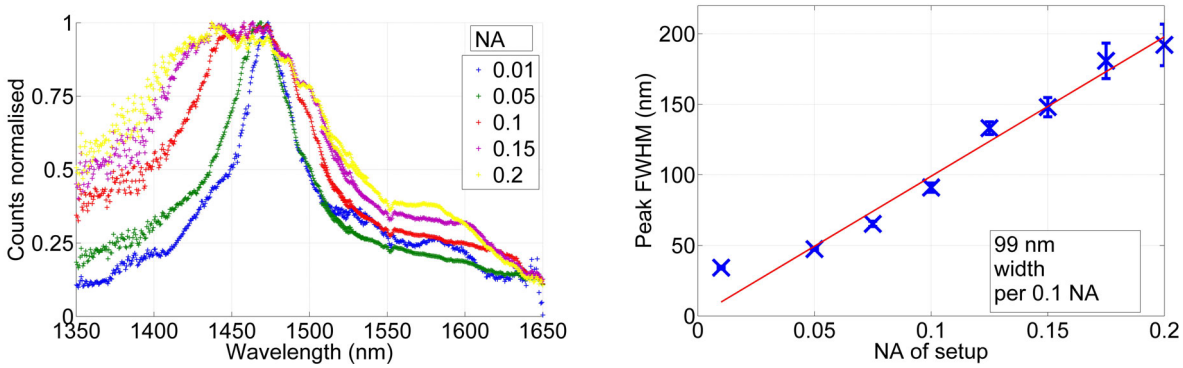

(a) (b)

Figure 5.1: *Figure (a) shows the spectrum of the sample with 500 nm slit spacing measured with different NA. A decrease in NA leads to narrowing of the peak. Figure (b) shows the FWHM of the fluorescence peak at different NA.*

By moving the pinhole parallel to the polarisation, as shown in figure 5.2(a), a different angle is selected. Figure 5.2(b) shows the spectrum of the 500 nm spacing slit array measured at different angles. All the following angle changing

measurements were made using the standard settings at 260 mW power and with an NA of 0.05.

The spectrum where the pinhole is almost in the centre (yellow) shows one modest peak around 1530 nm. When increasing the angle, the peak splits in two and continues to move away from the central resonant wavelength. The peak becomes smaller at the edges of the fluorescence and once it has moved out of the fluorescence range it disappears.

If the pinhole is moved perpendicularly to the optical polarisation, parallel to the slits, no difference in the measured spectrum is seen.

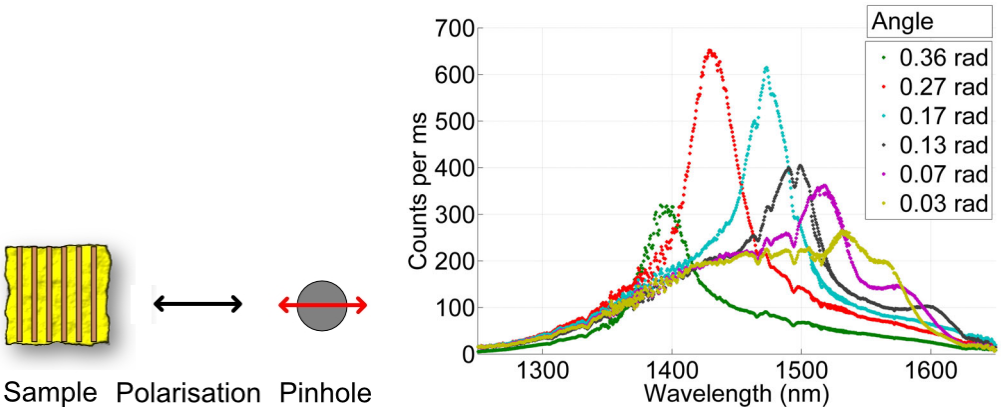

(a) (b)

Figure 5.2: *Figure (a) shows the direction of the pinhole movement. Figure (b) shows the spectrum of the 500 nm slits measured at different angles using 260 mW power and an NA of 0.05. The feature splits and the two halves move with the changing angle.*

In figure 5.3 the same measurement is shown for the 500 nm spacing hole array. At normal incidence three peaks are found in the measurement. The first peak is small with its maximum at 1460 nm. From the transmission simulations it is deduced that this peak is probably related to a plasmon resonance in the (1,1) mode.

The other two peaks around 1580 nm partially overlap. At this wavelength a small Rayleigh anomaly is seen in the transmission simulations, indicating that

these peaks are Rayleigh anomalies. Why this double peak is observed is not understood. Surprisingly the peak is more clearly visible in the fluorescence measurement, then in the linear transmission data.

The behaviour of the peaks in figure 5.3 is the same as in the measurement with the slit array in figure 5.2(b). When increasing the angle the peaks split up and move. The double peak on the Rayleigh anomaly becomes a single peak in the spectrum measured at larger angles when the second peak presumably shifts beyond the band gap.

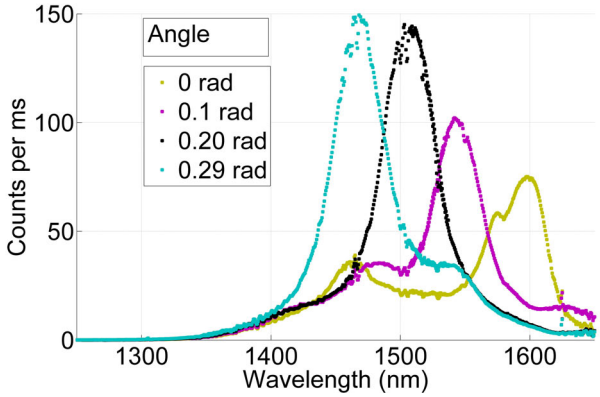

Figure 5.3: *The spectrum of the 500 nm spacing hole array measured at different angles, using 260 mW power and an NA of 0.05. At normal incidence (yellow) two features can be seen. The small feature is the plasmon resonance and the big feature with a double peak is a Rayleigh anomaly. The features show the same behaviour as in figure 5.2(b).*

To prove that the peak around 1460 nm is in the (1,1) plasmon mode, the polarisation angle and pinhole movement direction are changed as illustrated in figure 5.4(a). The selected polarisation is at 45 degree's from the hole array and the pinhole is moved perpendicularly to the polarisation. With this configuration the plasmons that propagate along the polarisation angle are selected.

In the resulting spectrum, shown in figure 5.4(b), the large Rayleigh anomaly peak moves while the plasmon peak remains stationary, indicating that the plasmon peak is in the (1,1) mode.

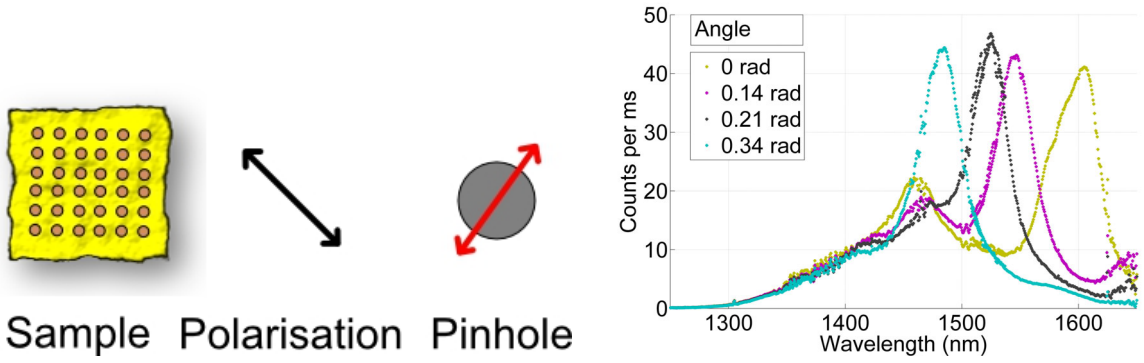

(a) (b)

Figure 5.4: *Figure (a) shows the direction of the pinhole movement for testing if the 1460 nm peak is due to the (1,1) plasmon mode. Figure (b) shows the same measurement as figure 5.3, but with the modified movement direction. The small plasmon peak remains stationary.*

By plotting the positions of the peak as function of the sine of the angle the sample spacing and the central wavelength of the peak can be accurately determined.

All peak positions move linearly with the sine of the angle. The Rayleigh anomaly (blue) of the slit array intersects the axis at a smaller wavelength than the Rayleigh anomaly of the hole array.

These positions are fitted with a line to find the slope and the the position where the line intersects the y-axis. Examples of these plots can be found in figure 5.5.

The slope found from the fit, should equal the spacing of the array structure. This can be seen by deriving equation 2.1 to $\sin(\theta)$. However the sample spacing determined from the slope is often found to be smaller than expected. This could be due to plasmons with a different wavelengths getting another phase shift when coupling out.

The intersection point with the y-axis is used to accurately determine the effective index. At this point the measurement angle is zero, and the effective mode index is found by dividing the wavelength at the intersection point by the

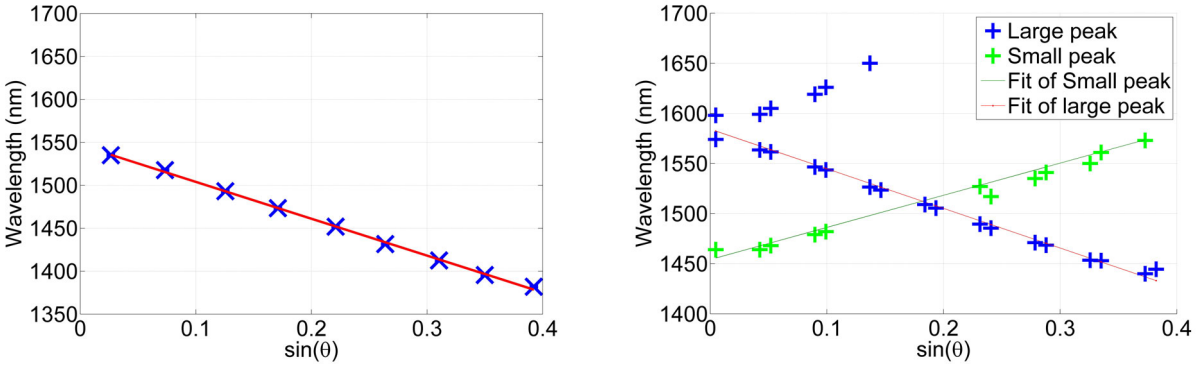

(a) (b)

Figure 5.5: *The positions of the peaks as a function of the sine of the angle. Figure (a) shows the position of the Rayleigh anomaly for the 500 nm spacing slit array. Figure (b) illustrates the results for the 500 nm spacing hole array with the Rayleigh anomaly (blue) and the plasmon feature (green).*

	Spacing (nm)	Spacing from slope (nm)	Centre λ (nm)	Effective index
Slits	400	410 ± 63	1288	3.22
	500	460 ± 60	1540	3.08
	800	820 ± 63	1318	3.30
Holes	400	341 ± 44	1335	3.34
	500	566 ± 44	1584	3.17
(1,1) mode	500	458 ± 63	1454	4.11

Table 5.1: *Effective index of the features calculated from the change in peak position using formula 2.1.*

sample spacing, as seen from equation 2.1. In table 5.1 an overview of the effective indexes of the samples can be found. The error on the index is less than 2%.

The effective index of 4.11 for the (1,1) mode is closer to the value expected for a plasmon than the value of 4.6 found in the linear transmission for the (2,0) mode with 500 nm spacing. However, this mode experiences a different hole density, which would partly explain the increased index.

The effective index of the Rayleigh anomaly with a hole array, is higher than that of the slits. There is no obvious dependency of the effective index and the array spacing.

As discussed in chapter 2, the amount of gain is wavelength dependent. A maximum is expected near the Fermi level. Therefore, the propagation length is

expected to change with the wavelength.

Using the fitting procedure we can find the propagation length for the different features. In figure 5.6, the propagation length of the Rayleigh feature of the 500 nm spacing slit array, is shown. The expected change is not observed. A possible explanation for the absence of change may be that the Rayleigh anomalies are caused by a lossy wave guide mode that is primarily in the substrate, thus they are not effected by the gain from the InGaAs layer.

Unfortunately this measurement can not be done for the (1,1) mode peak shown in figure 5.3. Upon varying the angle, the Rayleigh peak starts to overlap with the plasmon peak.

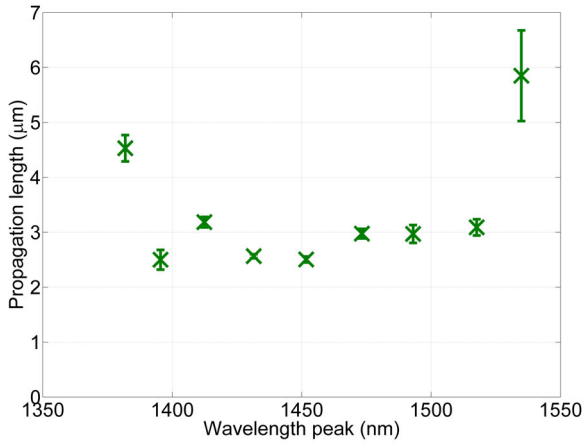

Figure 5.6: *Propagation length plotted against the location of the Rayleigh anomaly in the 500 nm spacing slit structure. No significant change is seen.*

5.2 Changing pump power

When increasing the pump power the losses of the plasmon in the InGaAs layer should decrease. If the power can be increased further, the layer should become transparent for the plasmons and eventually even result in gain. Thus an increase in propagation length is expected with higher pump power.

If there is gain, lasing might occur due to the reflection at the structures in the gold. Lasing occurs when more output is seen from stimulated instead of

spontaneous emission. Lasing can be recognised from clamping; this means that despite an increase in power no spectral band filling occurs but all extra power goes into stimulated emission.

For the measurements as function of the pump powers, the spectra were measured using an NA of 0.05 and a pump spot with a FWHM of 10 μm. With these settings the FWHM does not decrease when increasing the pump spot at maximum pump power, thus the FWHM is limited by the losses only.

The resulting spectra for the different arrays are shown in figure 5.7. Figure (a) is taken for the 500 nm spacing slit array measured at an angle of 0.1 rad. The peak is a Rayleigh anomaly. Figure (b) shows the results for the 500 nm spacing hole array at an angle of 0.07 rad. The small feature seen at 1460 nm is the plasmon resonance, the large peak at 1580 nm is the Rayleigh anomaly.

The fluorescence spectra show the same behaviour as the spectra measured with a large NA. There is increased band filling with higher power and features appear once the fluorescence has reached small enough wavelengths.

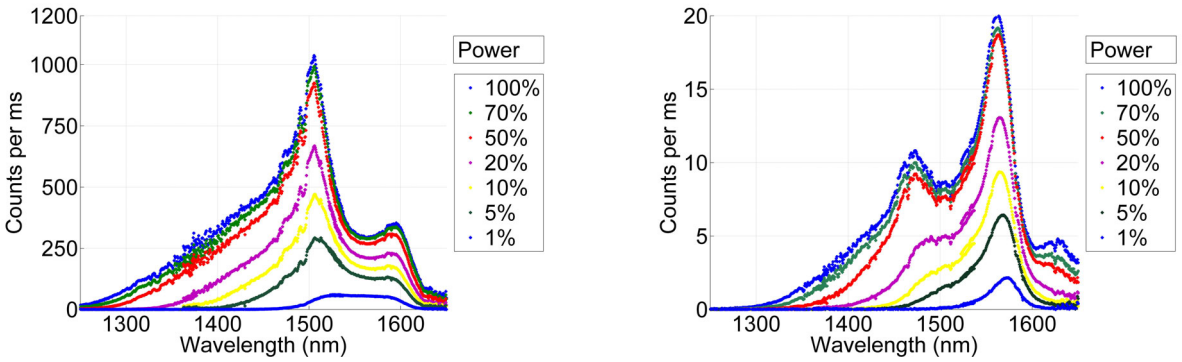

(a) slits (b) *holes*

Figure 5.7: *Fluorescence spectrum measured with different pump powers using a narrow NA of 0.05. 100% pump power corresponds to 260 mW. Figure (a) is the 500 nm spacing slit array at an angle of 0.1 rad. The peak seen is a Rayleigh anomaly. Figure (b) shows the 500 nm spacing hole array at an angle of 0.07 rad. The peak seen at 1460 nm is the plasmon resonance, the larger peak at 1580 nm is the Rayleigh anomaly.*

To visualise a possible clamping effect, the amount of counts in the Rayleigh peak is compared to the number of counts in the rest of the spectrum. If there is clamping, more power should go to the features than to the band filling. By

integrating the Lorentzian and fluorescence terms of the fit, an estimation of the amount of counts is made.

Figure 5.8 shows the amount of counts at different pump powers for the 500 nm spacing slit sample shown in figure 5.7(a). The result is similar to that obtained by of M.T. Hill for metallic-coated nanocavities [5]. The amount of power the fluorescence shape gains with an increase in power decreases once the feature appears, indicating there is some clamping.

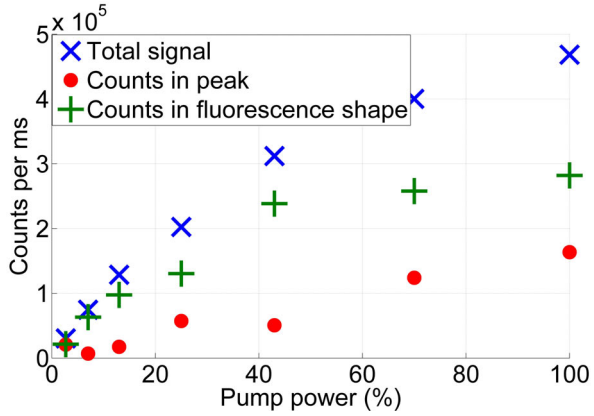

Figure 5.8: *The count distribution at different pump power of the 500 nm spacing slit sample. Blue is the total amount of counts, green is the amount of counts in the fluorescence and red is the for the Lorentzian.*

In figure 5.9 the propagation length of the feature is shown as a function of the pump power. This propagation length is found from the fit of the measurements shown in figure 5.7. Both the Rayleigh and plasmon features of the 500 nm spacing slit and hole arrays have a propagation length of roughly 3 μm at all pump powers. However, at pump powers, smaller than 20%, the plasmon feature is not clearly visible, making the fit unreliable; The error bars for these low powers are probably underestimated.

The propagation length for the plasmon may have increased during the first 20% power increase, however a further increase has little effect on the propagation length. A possible explaination is that since the extra power increases the temperature, the power mainly goes to more bandfilling instead of extra gain.

A propagation length of 3 μm is of the same order of magnitude as propagation

lengths found for samples without a gain layer, indicating that pumping the gain layer has made it more transparent.

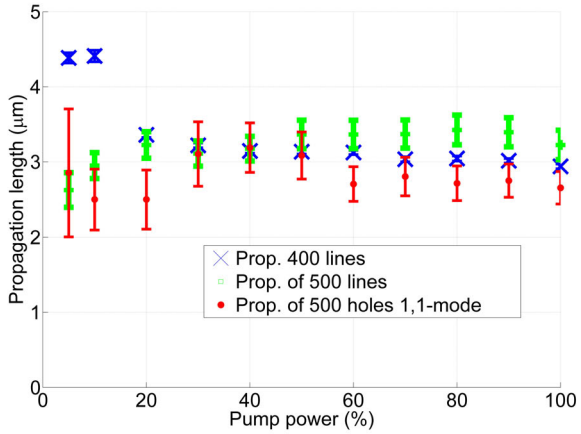

Figure 5.9: *The propagation length of the features as function of the pump power for features of the 400 nm(blue)/500 nm(green) slits and the (1,1) plasmon mode feature in the 500 nm(red) spacing hole array.*

5.3 Polarisation dependence

Since plasmon features only exist in a TM mode they should disappear when measuring with a different polarisation. The Rayleigh anomalies may also have a polarisation dependence. Polarisation measurements have been performed both for the linear transmission measurements and the fluorescence measurements.

Light can change polarisation during transmission due to rough edges of the structures. This depolarisation is quantified by measuring the linear transmission with crossed polarisers. Independent of the orientation of the sample, the measured signal with these crossed polarisers is more than three orders in magnitude lower than the signal measured with parallel polarisers. Thus both the slits and holes do not depolarise the light more than 0.1%.

Linear transmission measurements can be done for the slit arrays with both input and output polarisers positioned parallel to the slits, as shown in figure

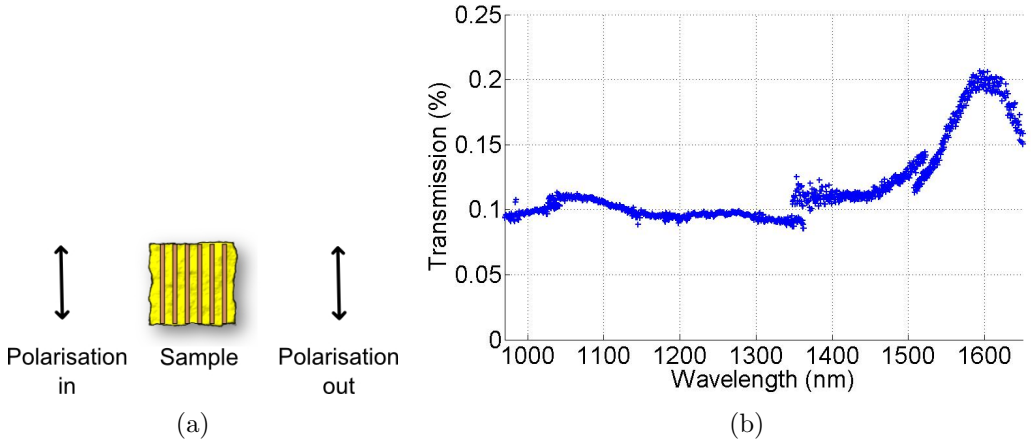

Figure 5.10: *Figure (a) shows the non-standard polarisation direction for linear transmission used to measure the transmission of the 500 nm spacing slit array shown in figure (b).*

5.10(a). The resulting transmission, presented in figure 5.10(b), is generally an order in magnitude smaller, since sub-wavelength arrays transmit light better in the perpendicular direction.

The resulting spectrum has a peak at 1600 nm, in contrast to the 1550 nm found in the regular linear transmission measurement (see figure 4.1C). This change in wavelength is not yet understood. Since the centre wavelength of 1600nm gives an effective mode index of the substrate and no plasmon peaks have been seen with slit arrays, the peak can be identified as a Rayleigh anomaly.

Polarisation measurement using fluorescence can only be carried out with the slit arrays, since the input polarisation cannot be selected. Thus spectra of the hole arrays are polarisation independent.

In figure 5.11 the fluorescence spectrum of the 400 nm spacing slit array, is shown with polarisations horizontal and perpendicular to the slit array. To compare the shape they are normalised. However, the fluorescence signal measured with parallel polariser is 20 times smaller than that of the perpendicular polarisers. Since the depolarisation could only account for less than 0.1% the spectrum is almost completly from parallel polarised light. The two spectra have a similar

shape and the Rayleigh feature is still visible.

Since Rayleigh anomalies are seen with both polarisations it is likely they are independent of polarisation, as predicted by the literature [9].

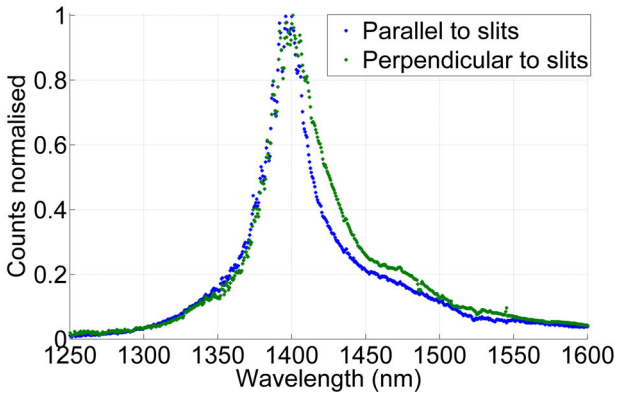

Figure 5.11: *Spectra of the 400 nm spacing slit array with 260 mW power and an NA of 0.05 measured with polariser parallel(blue) and perpendicularly(green) to the slit arrays. The shape of the spectra are similar and both have a Rayleigh anomaly feature. However, the absolute power observed is a factor 20 lower for the parallel polaristation.*

Chapter 6

Conclusion

The goal of this research was to investigate if adding a gain material to a metal surface could increase plasmon propagation length. The gain material was optically pumped using a laser with 1064 nm wavelength. Due to spontaneous emission in the gain layer plasmons could be excited. Through the process of stimulated emission these plasmons experienced a gain. These plasmons were studied by coupling them out through a periodic structure in the gold, and by measuring the resulting emission spectrum.

The periodic structures caused resonances to appear in the linear transmission of the samples. Resonances caused by Rayleigh anomaly and plasmons were identified from the peak position in measurements and simulations. However, the slit arrays only showed Rayleigh features, indicating that the plasmon losses from these structures were still too high.

The spectrum of the fluorescence resulting from optical pumping was comparable to theory. Furthermore, the periodic structure in the gold caused plasmon and Rayleigh resonances also to appear in the fluorescence spectrum.

These resonances were studied by changing the measurement angle. This resulted in a change of the centre wavelength of the resonances. Since the amount of gain is wavelength dependent, a change in the propagation length should have been observed. However, due to the spectral overlap of the Rayleigh and plasmon resonance, this change could not be measured. The amount of pump power should also lead to a change in the amount of gain and propagation length. Again this change could not be seen clearly.

The idea of putting a gain material onto a piece of metal to increase the propagation length of plasmons has potential. A propagation length of 3 μm has been measured when pumping the InGaAs layer. This length is comparable to the propagation lengths calculated for a transparent InGaAs layer. Numerous improve-

ments can still be made to increase the propagation length. These improvements are discussed in the outlook.

Chapter 7

Outlook

Before plasmons with a longer propagation length can be found in our samples, the amount of loss needs to be reduced. There are at least three different approaches to decreasing this loss. The loss may be reduced by omitting the plasmon absorbing chromium layer used to stick the gold to the InGaAs. Changing the spacing of the structures, using fewer slits and holes, will reduce the out-coupling of plasmons and therefore also minimise the loss. Finally, the out-coupling loss could also be reduced by decreasing the refractive index encountered at an aperture in the gold. This could be done by filling the openings with another material.

Another challenge is to accurately measure the longer propagation lengths. For this, the NA of the collection optics, needs to be decreased so sharper peaks can be measured. However, a smaller NA would decrease the signal and the spatial resolution. A change in the amount of slits would also reduce the signal. This can be compensated by increasing the sample size, or by using a more sensitive camera.

For making future plasmon lasers a slit structure can be used. Since plasmons partly reflect at structures in the gold, this would have a similar effect as a fibre Bragg grating in distributed feedback lasers. However, the ratio between reflection and loss will need to be improved.

Chapter 8

Acknowledgments

I would like to thank Martin van Exter and Frerik van Beijnum of the QO- group for offering me the opportunity to perform my research project and for their constructive guidance and advice. Also I would like to thank Jeroen Sirre for his company and Wolfgang Löffler for helping me when Frerik was not available. Furthermore, the discussions with Gert 't Hooft have greatly helped me with the interpretation of the results. Working with the Quantum Optics group of the University of Leiden has been a very instructive and most enjoyable experience.

Bibliography

[1] R.H. Ritchie, Physical Review 106 (5): 87488 (1957)

[2] R.H. Ritchie, E.T. Arakawa, J.J. Cowan, R.N. Hamm, Physical Review Letters 21, no. 22, pp.1530 (1968)

[3] T. W. Ebbesen et al., Nature (London) 391, 667 (1998)

[4] M. Fleischmanna, P.J. Hendraa and A.J. McQuillana, Chemical Physics Letters, 26, Issue 2, pp. 163-166 (1974)

[5] Martin T. Hill (et al.), Nature Photonics 1, pp.589-594 (2007)

[6] J. A. Hutchison, D. M. O'Carroll, T. Schwartz, C. Genet, T. W. Ebbesen, Angewandte Chemie International Edition 50, 2085-9 (2011)

[7] S. Pillai, K. R. Catchpole, T. Trupke and M. A. Green, J. Appl. Phys. 101 (9): 093105. (2007)

[8] Haitao Liu, Philippe Lalanne, Nature 452, 728-731(2008)

[9] A. Hessel and A. A. Oliner, Appl. Opt. 4, 1275-1297 (1965)

[10] K. Peterman, Laser diode modulation and noise, (Kluwer Academic Publishers, 1988)

[11] Raether, H. Surface Plasmons on smooth and rough surfaces and on gratings, (Springer-Verlag1988)

[12] Edward D. Palik, Handbook of Optical Constants of Solids, (Academic Press, 1985)

[13] S.Adachi, Physical Properties of III-Y Semiconductor compounds. John Wiley and Sons.1992

[14] E.Zielinski, H.Schweizer, K.Streubel, H.Eisele, G.Weimann, J. Appl. Phys. 59, no.6, pp.2196-2204(1986)

[15] Yeh P., Optical waves in layered media, (Wiley Interscience, 1988)

[16] Y. P. Varshni, Physica 3, 149 (1967)

[17] K-H. Goetz, D. Bimberg, H. Jurgensen, J. Selders, A.V.Solomonov, G.F.Glinskii, M. Razeghi, J. Appl. Phys., 54, 4543-4552 (1983)

[18] Glazov, V. M., K. Davletov, A. Ya. Nashelskii, and M. M. Mamedov, Zh. Fiz. Khim. 51, 2558-2561 (1977)

[19] Goldberg Yu.A. and N.M. Schmidt Handbook Series on Semiconductor Parameters, vol.2, M. Levinshtein, S. Rumyantsev and M. Shur, ed. (World Scientific, London, 1999)

[20] C. Smiet , Plasmonics in metal hole arrays, bachelor report, (Leiden University, 2010)

[21] Aliev, S. A., A. Ya. Nashelskii, and S. S. Shalyt, Sov. Phys. Solid State 7, 1287 (1965)

[22] J.D.Oliver, Jr., L.F.Eastman, P.D.Kirchner, W.J.Schaff, J.Cryst.Growth., 54, no.1, pp.64-68 (1981)

[23] J.Novak, M.Kuliffayova, M.Morvic, P.Kordos, J.Cryst.Growth, 96, 645-648 (1989)

[24] Curtis J. Humphrys, The Sixth Series in the Hydrogen Spectrum, J. Opt. Soc. Am. 42, 432-432 (1952)